# Fluid pinch-off in superfluid and normal $^4$He

J. C. Burton, J. E. Rutledge, and P. Taborek
*Department of Physics and Astronomy, University of California, Irvine, California 92697-4575, USA*
(Received 25 October 2006; published 26 March 2007)

We present frames from high-speed videos of the pinch-off of liquid $^4$He droplets. The temperature of the fluid droplets ranged from 1.33 K to 4.8 K, and the size of the drops was proportional to the temperature-dependent capillary length. We observed no qualitative difference between pinch-off in the normal and superfluid states. In both cases, the shape of the fluid in the final stages of pinch-off resembles a cone piercing a sphere, which is typical of other low-viscosity fluids. The evolution of the minimum neck radius $r_{min}$ can be characterized by power laws $r_{min} \propto \tau^n$, where $\tau$ is the time remaining until pinch-off occurs. In the regime near pinch-off, the data from image analysis are consistent with $n=2/3$. The data at the beginning of the pinch process when the neck is of the order of the capillary length are also described by $n=2/3$, but with a different proportionality factor. There is an intermediate crossover regime characterized by $n=2/5$.

DOI: 10.1103/PhysRevE.75.036311 PACS number(s): 47.55.df, 67.55.Fa, 67.57.De

## I. INTRODUCTION

The capillary breakup of one droplet into two pieces is a particularly simple physical system which spontaneously forms a singularity. Quantities such as pressure and velocity diverge near the singularity while length scales approach zero. The minimum neck radius of the pinching region typically follows a power-law behavior in the time remaining until the singularity is reached, $r_{min} \propto \tau^n$, where the exponent $n$ is between 0 and 1. The structure and dynamics of the singularity depend on the relevant fluid properties and possibly on the initial conditions. Recent research has focused on free-surface singularities in simple Newtonian fluids [1–6], as well as more complex fluids including drops covered with surfactants [7,8], polymers [9,10], and quantum solids and fluids [11,12]. Superfluids are a distinctly different class of fluid, with many unusual properties. In many respects, a superfluid is the closest realization to an ideal inviscid fluid, which is a consequence of the vanishing viscosity in the superfluid state. For low-viscosity fluids, the exponent $n$ in the above scaling law is expected to be equal to 2/3, which has been numerically verified [13–15]. Recent experimental data using high-speed video [15] to study low-viscosity pinch-off in water droplets is consistent with $n=2/3$, but the reentrant profile of the pinch region obscures the singularity from optical access. Measurements using high-speed electronics to monitor pinch-off in liquid mercury have shown that the 2/3 power law persists to atomic dimensions [16]. The purpose of the research reported here is to optically investigate pinch-off in superfluid and normal $^4$He and to explore possible effects of the unusual flow properties of superfluids on the pinch-off process.

At the λ point at $T=2.1768$ K, $^4$He undergoes a phase transition into a superfluid state which is phenomenologically described by a two-fluid model in which the superfluid and normal components coexist, and the relative superfluid fraction increases toward unity as the temperature approaches zero. Some nonclassical flow effects that could affect the behavior of the pinch-off include the thermomechanical effect, quantized vortices, and the existence of a critical velocity. The superfluid thermomechanical effect describes the strong coupling that exists in superfluids between temperature gradients and pressure gradients. For example, heat is not transported by diffusion in superfluid $^4$He because even small temperature gradients induce large flows in both the superfluid and normal components which rapidly reduce the temperature gradient to zero. The quantum mechanical nature of superfluid requires that the vorticity of superfluid be quantized in the form of nanometer-sized vortices, which have recently been visualized using optical methods [17]. These vortices usually nucleate on the walls of the container or on impurities. Very little is known, however, about the nucleation of vortices on a moving free surface without solid boundaries. Dissipationless superflow is possible only below a critical velocity that depends on the geometry of the flow. Above this critical velocity, elementary excitations are spontaneously created and lead to breakdown of the superfluid. Since velocities diverge near the singularity during fluid pinch-off, the presence of a critical velocity could possibly affect the flow at some stage of pinch-off. The liquid-vapor surface tension is a smooth and continuous function of temperature [18] through the λ point, but curvature also generates a pressure discontinuity through the Laplace effect, which can drive evaporation and flows of latent heat. At a highly curved interface near a singularity, these effects could become large enough to visibly affect the dynamics of pinch-off.

## II. EXPERIMENTAL METHODS

The primary data of our experiments consist of high-speed photographs of liquid helium dripping from the end of a solid cone-shaped surface; a typical example for a superfluid droplet is shown in Fig. 1. The photographs were taken in a special purpose custom-made optical cryostat similar to that used in previous superfluid experiments in our laboratory [19,20]. This cryostat has two separate reservoirs, one for liquid nitrogen and one for liquid helium. Each reservoir is attached to a radiation shield that surrounds the experiment, protecting it from the room-temperature infrared radiation from the outer vacuum can as shown in Fig. 2.

 

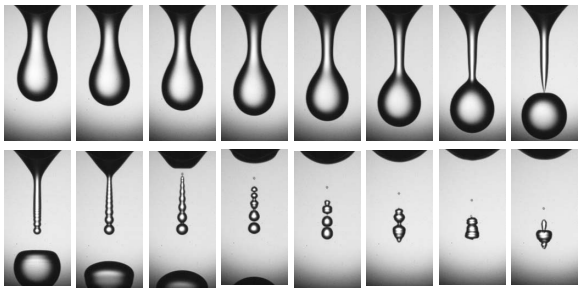

FIG. 1. Sequence of frames taken from a high-speed video showing the pinch-off of a superfluid droplet at 1.34 K. The time between individual frames is 1.22 ms. The exposure time of each frame was 15 $\mu$s. After pinch-off occurs, the remaining filament is subject to a capillary instability and eventually pinches off again near the top of the picture. The remaining satellite drop rebounds and undergoes large oscillations as it falls under the influence of gravity. The liquid drop is approximately 1 mm in diameter and is surrounded by helium vapor at the saturated vapor pressure, which is 1.56 Torr.

At atmospheric pressure, $^4$He boils at 4.2 K. To obtain temperatures below the λ point, we used a continuous-flow refrigerator consisting of a copper pot equipped with a pumping line to reduce the vapor pressure and a filling capillary which delivered liquid from the bath, as shown in Fig. 3. The impedance of this capillary was $1.4\times10^{11}$ cm$^{-3}$. The subsequent evaporation of the liquid cools the experimental cell. A copper condenser containing sintered copper pellets was used to liquify $^4$He gas to form a reservoir of liquid at the temperature of the cell which was used as a source to form droplets. The liquid entered the cell through another capillary of impedance $1.1\times10^{12}$ cm$^{-3}$. The liquid dripped into a copper colander inside the cell and then drained onto the end of a rounded copper cone ~0.5 mm in radius. This method ensured that the drops were not affected by pressure fluctuations in the incoming capillary tube and that a large amount of liquid could collect, producing the largest droplets possible. The drip rate was controlled using a needle valve connected to a pressured tank of $^4$He gas, and drips occurred about once every 10 s.

Our first attempt at imaging superfluid pinch-off used laser-triggered still photography [Fig. 2(a)], the initial results of which were published in Ref. [20]. In this experiment, a 1-Mpixel Kodak DCS 315 digital camera was attached to a long-range microscope (Infinity K2), with a focal distance of approximately 25 cm. This configuration corresponded to an optical resolution of 3 $\mu$m per pixel. A rectangular piece of blue glass was inserted in front of the camera and oriented at an angle of 45° from the optical axis. This glass was used to reflect a beam from a 632-nm red diode laser down the axis of the microscope and through the cryostat; it also prevented scattered or reflected red laser light from entering the camera. The intensity of the laser was detected on the opposite side of the cryostat with a photodiode. The laser beam was positioned just under the drop so that when the beam was interrupted, the voltage on the photodiode was reduced which triggered a delay-pulse generator (Berkeley Nucleonics model 555). The pulse generator then triggered a flash circuit connected to a standard xenon bulb. The width of the

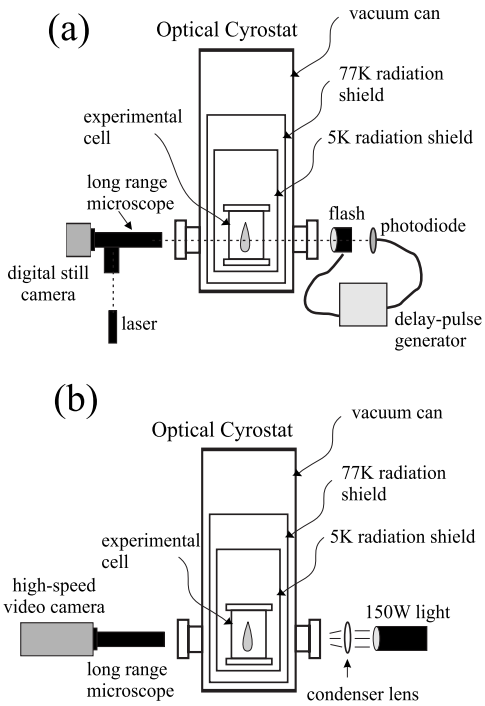


FIG. 2. (a) Schematic of the optical cryostat used to view dripping $^4$He droplets using laser-triggered still photography (a) and high-speed video (b). The sealed experimental cell is thermally isolated by two coaxial radiation shields. These shields contain windows with infrared absorbing glass, which blocks the majority of heat from the flash or spotlight. The optical setup for (a) consisted of a diode laser made to pass into the microscope and reflect off of a piece of blue filter glass, and then pass through the cryostat to the photodiode. When the drop interrupts the beam, the delay-pulse generator is triggered, which subsequently triggers the flash for the still digital camera. The optical setup for (b) uses a high-speed video camera to image the drop through the microscope using a bright spotlight. To obtain illumination necessary for high-speed video, a condensing lens was used to focus the light.

flash was approximately 5 $\mu$s. The delay between the initial trigger from the photodiode and the trigger sent to the flash could be controlled on the pulse generator with a resolution of 1 ns. Pictures were taken of successive droplets, with the the delay adjusted to obtain data at different values of $\tau$. The short duration and low duty cycle of the illumination pulses used in the laser triggered measurements ensured that the heat load on the experiment was extremely low, which is the principal advantage of this technique. The pictures could be assembled into a movie, but it is important to note that every frame of this stroboscopic movie corresponds to a different drop recorded at longer and longer time delays from the triggering event. This synthetic movie will faithfully reproduce the evolution of a single pinch-off only if the triggering is absolutely stable and the drops are all identical. Because the laser and microscope must be located outside the cryostat, there is a lever arm of almost 50 cm between the laser and the forming drop. Small vibrations of the cryostat and optics cause jitter in the location of the laser beam relative to the dripper. The spatial jitter results in timing errors that are responsible for the considerable scatter seen in the data in Fig. 4.

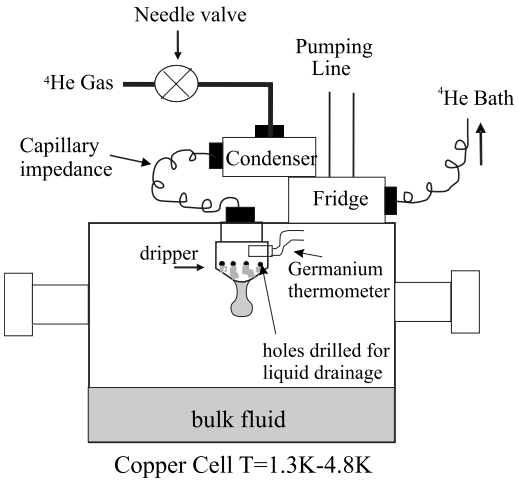


FIG. 3. Schematic of the experimental cell used to create superfluid droplets. The fridge was cooled by evaporation of $^4$He. The drip rate was controlled by adjustment of a needle valve connected to a pressured source of $^4$He gas. The liquid condenser was attached directly to the refrigerator to ensure that the drops are in thermal equilibrium with the cell. A capillary impedance connected the condenser to the dripper in the cell. At the end of the condenser in the cell, a copper cup with holes drilled in it collected the liquid and drained it to the end of a round copper tip ~0.5 mm in radius, where the drop formed and eventually pinched off. The germanium thermometer was inserted into the side of the cup to measure the temperature near the source of the droplets.

Because of the scattered data it produced, the laser triggering technique was abandoned in favor of high-speed videography which could record the evolution of a single drop. A potential disadvantage of video is that it requires continuous illumination rather than a strobe flash, so the heat load on the cryogenic system is higher. A Phantom V7.1 high-speed camera (Vision Research) was used to take videos of the drops at frame rates up to 47433 fps. The high-speed camera was attached to the long-range microscope to image the droplets [Fig. 2(b)]. The maximum image size possible was $800 \times 600$ pixels, which corresponded to an optical resolution of 8.85 $\mu$m per pixel. To capture sharp images of the drop, an exposure time of 15 $\mu$s was set on the camera. Shorter exposure times required higher-intensity illumination, which induced significant heating of the system. However, a 15-$\mu$s exposure still required fairly bright light.

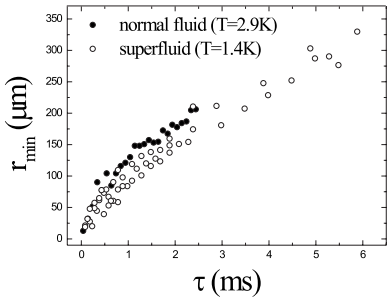


FIG. 4. Data obtained using laser-triggered still photography of $r_{min}$ vs $\tau$ for one normal and one superfluid droplet. The large scatter in the data is mostly due to slight variations in the laser position.

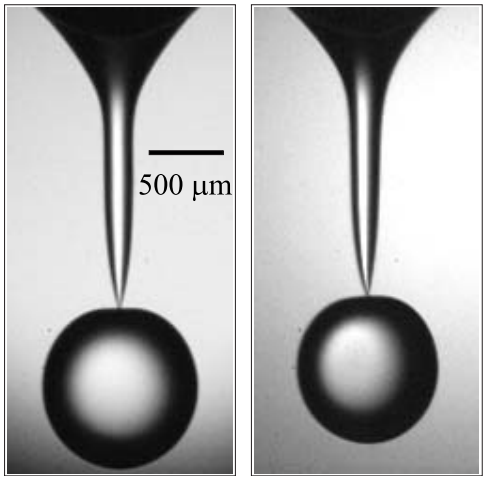


FIG. 5. Photographs taken from digital videos showing the pinch-off of a superfluid at $T=1.34$ K (left) and normal $T=2.32$ K (right) droplet. The difference in the size of the drops is due to the temperature dependence of the capillary length. There is, however, no noticeable qualitative difference between the shapes of the two drops, as both pinch off like an ideal inviscid fluid on length scales above optical resolution.

The windows on the radiation shields were made from KG1 Schott glass, which had a transmittance of approximately $10^{-5}$ in the far infrared. This glass served to filter out most of the infrared heat from the illumination. A four-wire germanium thermometer was placed right above the copper dripper to measure the temperature of the droplet and to observe the effects of heating due to the illumination. At full power, the light raised the lowest temperature of this thermometer from 1.30 K to 1.34 K, with no observable effects in the droplet pinch-off.

## III. RESULTS

Figure 5 shows a comparison of a superfluid and normal droplet at the moment of pinch-off. The temperature of the drops was 1.34 K and 2.32 K, respectively. The superfluid fraction at 1.34 K is 94.5%, so the drop on the left in Fig. 5 is almost entirely superfluid. The shape of each pinch-off is that of a cone piercing a sphere, which is characteristic of inviscid pinch-off. There is no qualitative difference in the geometry of the pinch-off in the two pictures, and they are both consistent with the pinch-off of other low viscosity fluids such as water. The difference in size of the two droplets in Fig. 5 is due to the temperature dependence of the capillary length of liquid helium, $l_g=\sqrt{\sigma/\rho g}$, where $\sigma$ and $\rho$ are the surface tension and density of the liquid, respectively, and $g$ is the acceleration due to gravity. The capillary length is the length scale at which gravitational and capillary forces are in balance. The temperature dependence of the size of the droplets is most readily apparent in Fig. 6, which shows laser-triggered photographs of helium droplets shortly after the initial pinch-off event for a wider range of temperatures: 1.4 K, 2.9 K, and 4.8 K. In each case the drops are approximately $2l_g$ in diameter, which becomes smaller at high temperatures and would presumably shrink to zero at the critical

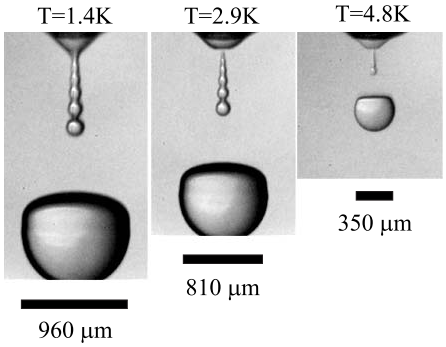


FIG. 6. Laser-triggered photographs showing $^4$He droplets shortly after pinch-off. The surface tension of $^4$He vanishes at the critical point $T=5.2$ K; thus the capillary length and droplet size become small. The bars indicate twice the capillary length $2l_g$ at the given temperature.

temperature of 5.2 K where the surface tension vanishes.

A quantitative comparison of pinch-off images to theory requires examining the behavior of the minimum neck radius $r_{min}$ as a function of the time remaining until pinch-off $\tau = t_o - t$, where $t_o$ is the time of pinch-off. A plot of $r_{min}$ vs $\tau$ for both superfluid and normal helium is shown in Fig. 7(a). The curves are similar but not identical. One reason for the difference is that the surface tension and density vary with temperature; therefore, it is more appropriate to plot the data as a function of dimensionless variables. The relevant dimensional parameters in our system are the surface tension $\sigma$, the

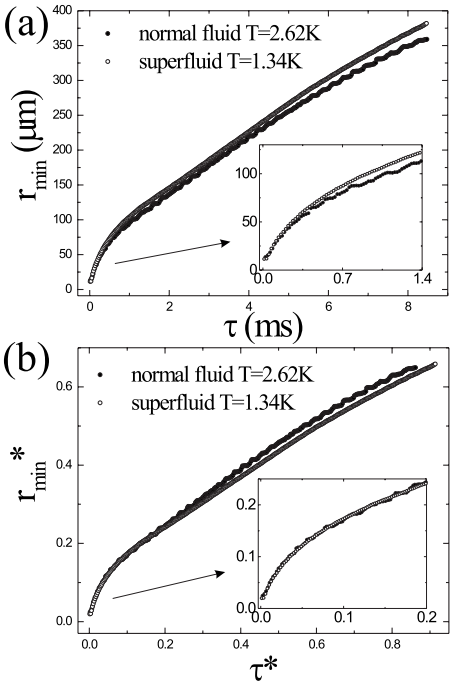


FIG. 7. (a) Raw data obtained from high-speed videos of $r_{min}$ vs $\tau$ for one normal and one superfluid droplet. (b) The same data plotted as a function of the dimensionless variables defined in Eq. (1). Far from pinch-off, the data do not collapse due to the differences in the gravitational bond number $G$ and the geometry of the dripper affecting the initial stages of pinch-off. The insets in both graphs show the same data plotted near the singularity.

fluid density $\rho$, the acceleration due to gravity $g$, and the characteristic drop radius $R$ at the moment of pinch-off. It is reasonable to assume that gravity will not affect the final stages of the breakup, since it is simply a body force and does not diverge near a finite-time singularity. Thus we choose $R$ as the length scale and the capillary time $t_c = \sqrt{\rho R^3/\sigma}$ as the time scale, resulting in the dimensionless variables

$$r_{min}^* = \frac{r_{min}}{R},$$

$$\tau^* = \frac{\tau}{\sqrt{\rho R^3/\sigma}}. \quad (1)$$

The remaining dimensionless group is known as the gravitational bond number, $G=(R/l_g)^2=g\rho R^2/\sigma$, which is a ratio of the gravitational to capillary forces in the system. Figure 7(b) shows data plotted using these dimensionless variables. For the superfluid drop at $T=1.34$ K, $R=0.53$ mm and $G=1.20$. For the normal fluid drop at $T=2.62$ K, $R=0.48$ mm and $G=1.31$. The fact that $G$ is of order 1 is not surprising since $R \sim l_g$, as indicated by Fig. 6. Far away from the singularity, the data do not collapse onto a single curve, which is most likely due to the fact that at early times properties such as the size of the conical dripper, details of the initial droplet geometry, and the bond number $G$ affect the flow.

The insets in Fig. 7 show the same data during the final stages of breakup. It may seem that the collapse of the data in this regime is quite good, which is not necessarily obvious. At times very near pinch-off, both theory [13,14,21] and experiment [16,15] show that the asymptotic scaling for $r_{min}^*$ becomes

$$r_{min}^* \propto \tau^{*2/3}. \quad (2)$$

Subsequently, the proportionality between $r_{min}$ and $\tau$ is $r_{min} \propto (\sigma\tau^2/\rho)^{1/3}$. Therefore, $R$ directly cancels out of the proportionality for the original variables $r_{min}$ and $\tau$. However, the constant of proportionality is still undetermined and would depend on the initial geometry and details leading up to pinch-off. Since the initial geometries of both the superfluid and normal droplets are nearly identical, it is not surprising that there is a collapse of the data in the inset of Fig. 7(b). The pinch-off of an inviscid fluid is a self-similar phenomenon with unique scaling exponents, but the constant of proportionality is not universal and unique as in the case of the pinch-off of a drop with viscosity, surface tension, and density, described by Eggers [22].

The log-log plot of $r_{min}^*$ vs $\tau^*$ in Fig. 8 shows that the data for the pinch-off of a superfluid drop near the singularity ($\tau^* \ll 1$) are consistent with a 2/3 power law. It should be noted that the choice of $t_0$ in Figs. 7 and 8 can have a large effect on the shape of the curves and the effective exponent which describes them, particularly in the region near $\tau^*=0$. We choose $t_o$ to lie halfway between the frame where the drop is still connected to the neck and the next frame when the drop had just detached from the neck. This choice of $t_0$ is also made difficult by the profile of the pinch region, which

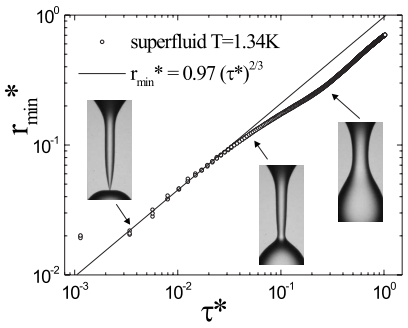


FIG. 8. $\mathrm{Log}_{10}$-$\log_{10}$ plot of scaled data from three separate superfluid pinch-off events. The photographs show the general shape of the droplets at the data points indicated by arrows. Data are consistent with a 2/3 power law near the singularity. The solid line indicates a 2/3 power law with a prefactor of 0.97. The last two data points appear to have the same neck size because the profile of the drop overturns at $r_{min} \sim 11$ $\mu$m.

is expected to be reentrant like that of the stem of an apple near the core [13–15]. The top of the drop forms a horizon which looks flat when viewed horizontally (Fig. 9), which hides the pinch-off point from view.

Another obvious difficulty in determining $t_o$ is the finite spatial and time resolution of the images. Figure 10 shows the ambiguities inherent in determining the power law that governs the minimum neck diameter. The figure shows four frames near the pinch-off event of a normal drop. First it is clear that the edges of the liquid are not sharp. A choice of grayscale threshold must be made to locate the edge of the drop. There is a range of plausible thresholds to choose from among these. The neck diameters deduced from the large end of this range are typically ~1.5 pixels larger than neck diameters deduced from smaller grayscale thresholds which corresponds to a range of about 13 $\mu$m. Second, as is seen in the figure, the first two images are nearly identical near the minimum and are probably unbroken. The bottom-right image (63 $\mu$s) appears to be definitely broken, and the bottom-left image (42 $\mu$s) is somewhere in between. All that can be said with certainty is that pinch-off occurred sometime between the second frame from the top and the bottom frame. This is a time span of 42 $\mu$s. Since the neck diameters are in

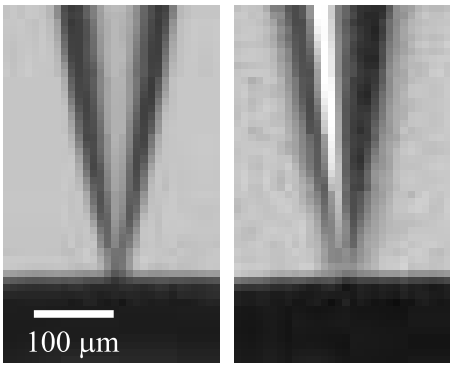


FIG. 9. High-magnification images of the pinching region for a superfluid $T=1.34$ K (left) and normal $T=2.32$ K (right) droplet. The shape of the pinch is that of a cone piercing a plate. The optical resolution is 8.85 $\mu$m per pixel.

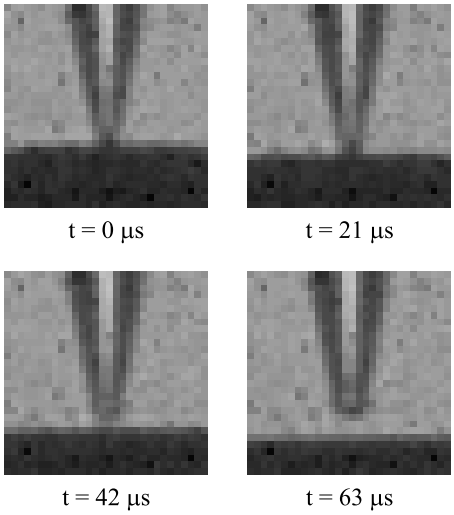


FIG. 10. Close-ups of the sequence of images of the pinching region for a normal droplet. The field of view is $265 \times 265$ $\mu$m$^2$. The choice for $\tau=0$ is rather ambiguous due to insufficient spatial and time resolutions. In the first two images (0 and 21 $\mu$s), the neck diameter is essentially the same, suggesting that the singularity has disappeared under the horizon. For this particular video, $\tau=o$ was chosen halfway inbetween the second and third frame, at $t_0 = 31.5$ $\mu$s.

the asymptotic limit for considerably less than one decade in $\tau$ or $r_{min}$, the exponent extracted from optical data is sensitive to the choice of the break time. In fact, depending on the choice of $t_0$ and the threshold grayscale value, the same set of data can appear to approach power laws with exponents in the range of 0.6–0.8. We believe all optical pinch-off experiments are similarly incapable of establishing the asymptotic behavior of inviscid pinch-off, and other experimental methods such as those described in Ref. [16] are necessary to study pinch-off in this regime.

The log-log plot of Fig. 8 exhibits straight power-law regions even for large values of $\tau^*$ where the shape of the fluid filament (shown in the inset photographs) more closely resembles a cylinder than a cone. It is interesting to note that even far from the singularity where the minimum neck radius is quite large, the data seem to follow a $r_{min}^* \propto \tau^{*2/3}$ power law, but with a different proportionality factor than in the singular asymptotic regime. There is also a transition region between this large $\tau^*$ behavior and the asymptotic $\tau^{*2/3}$ regime, illustrated by the middle photograph in Fig. 8. These features of the data can be explained by comparing our measurements to the numerical computations in Ref. [14], which investigates the pinch-off of an axisymmetric soap film bridge. Pinch-off in inviscid soap films is very similar to the pinch-off of axisymmetric inviscid droplets, with the same type of rentrant asymptotic profile, $\tau^{*2/3}$ scaling law, and similar cone angles near the singularity [13,23]. Chen and Steen [14] describe four distinct regimes of pinch-off. The data in Fig. 8 are consistent with three of these regimes, which they denote as "roll-off," "cusp approach," and "self-similar." The exponent $n$ predicted in the proportionality $r_{min}^* \propto \tau^{*n}$ for these three regimes is 2/3, 2/5, and 2/3, respectively. Figure 11 shows the data from Fig. 8 with dashed

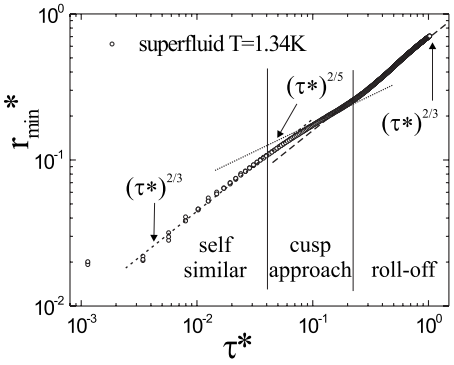


FIG. 11. $\text{Log}_{10}$-$\log_{10}$ plot of data from Fig. 8 plotted with dashed and dotted lines showing the three different regimes of inviscid pinch-off. Chen and Steen [14] numerically show that the "roll-off," "cusp approach," and "self-similar" regimes follow a power law $r_{min} \propto \tau^n$ where $n=2/3$, $2/5$, and $2/3$, respectively in each regime. The scaling laws are indicated by the dotted and dashed lines.

and dotted lines representing the three scaling laws. Although we do not observe the fourth regime, "onset," prior to the initial necking, we note that the numerical data presented in Ref. [14] describe a liquid bridge geometry rather than dripping due to gravity, and there is no reason to expect data from these to systems to be similar so early in the breakup process.

## IV. CONCLUSION

Pinch-off in liquid helium both above and below the λ point is very similar to other conventional low-viscosity fluids, with the same conical geometry and the same 2/3 scaling law of $r_{min}$ vs $\tau$. The size of the droplets scales with the temperature-dependent capillary length, which vanishes at the critical point. Far outside the asymptotic region where the fluid filaments are almost cylindrical, the $r_{min}$ vs $\tau$ data can also be described by a power law with a crossover regime. The flow regimes as well as the power-law exponents correspond closely with the calculations of [14]. Because of the ambiguities in the determination of the asymptotic power law, our strongest evidence for the lack of superfluid effects in the time range accessible to our measurement is the data shown in the inset to Fig. 7. The data there show that within the experimental resolution, the superfluid and normal fluid behave identically. This conclusion is independent of any assumptions about the mathematical form of $r_{min}$ as a function of $\tau$. Quantum effects could become important on submicron scales, but conventional photographic methods are not capable of probing this regime of inviscid pinch-off.

## ACKNOWLEDGMENTS

This work was supported by NSF Grant No. DMR 0509685.

[1] J. C. Burton, R. Waldrep, and P. Taborek, Phys. Rev. Lett. **94**, 184502 (2005).
[2] J. M. Gordillo, A. Sevilla, J. Rodriguez-Rodriguez, and C. Martinez-Bazan, Phys. Rev. Lett. **95**, 194501 (2005).
[3] J. Eggers, Rev. Mod. Phys. **69**, 865 (1997).
[4] I. Cohen and S. R. Nagel, Phys. Fluids **13**, 3533 (2001).
[5] A. Rothert, R. Richter, and I. Rehberg, Phys. Rev. Lett. **87**, 084501 (2001).
[6] P. Doshi, I. Cohen, W. Zhang, M. Siegel, P. Howell, O. A. Basaran, and S. R. Nagel, Science **302**, 1185 (2003).
[7] P. T. McGough and O. A. Basaran, Phys. Rev. Lett. **96**, 054502 (2005).
[8] Y. C. Liao, H. J. Subramani, E. I. Franses, and O. A. Basaran, Langmuir **20**, 9926 (2004).
[9] C. Wagner, Y. Amarouchene, D. Bonn, and J. Eggers, Phys. Rev. Lett. **95**, 164504 (2005).
[10] V. Tirtaatmadja, G. H. McKinley, and J. J. Cooper-White, Phys. Fluids **18**, 043101 (2006).
[11] R. Ishiguro, F. Graner, E. Rolley, and S. Balibar, Phys. Rev. Lett. **93**, 235301 (2004).
[12] H. J. Maris, Phys. Rev. E **67**, 066309 (2003).
[13] R. F. Day, E. J. Hinch, and J. R. Lister, Phys. Rev. Lett. **80**, 704 (1998).
[14] Y.-J. Chen and P. Steen, J. Fluid Mech. **341**, 245 (1997).
[15] A. U. Chen, P. K. Notz, and O. A. Basaran, Phys. Rev. Lett. **88**, 174501 (2002).
[16] J. C. Burton, J. E. Rutledge, and P. Taborek, Phys. Rev. Lett. **92**, 244505 (2004).
[17] G. P. Bewley, D. P. Lathrop, and K. R. Sreenivasan, Nature (London) **441**, 588 (2006).
[18] R. J. Donnelly and C. F. Barenghi, J. Phys. Chem. Ref. Data **27**, 1217 (1998).
[19] D. Ross, J. E. Rutledge, and P. Taborek, Science **278**, 664 (1997).
[20] J. C. Burton, P. Taborek, and J. E. Rutledge, J. Low Temp. Phys. **134**, 237 (2004).
[21] P. K. Notz, A. U. Chen, and O. A. Basaran, Phys. Fluids **13**, 549 (2001).
[22] J. Eggers, Phys. Rev. Lett. **71**, 3458 (1993).
[23] N. D. Robinson and P. H. Steen, J. Colloid Interface Sci. **241**, 448 (2001).